JOURNAL OF COMPUTATIONAL PHYSICS 76, 327–348 (1988)

On an Open Radiational Boundary Condition for Weakly Dispersive Tsunami Waves

KWANG Y. KIM,* ROBERT O. REID, AND ROBERT E. WHITAKER

Department of Oceanography, Texas A & M University, College Station, Texas 77843

Received October 31, 1986; revised June 17, 1987

A radiational condition compatible with a weakly dispersive governing equation for tsunami waves is developed for use at the open lateral boundaries of a limited-domain propagation model A Boussinesq-type governing equation for the interior is adopted. The resulting open boundary condition (OBC) is a modified Sommerfeld condition, in which the effects of weak dispersion, geometric spreading and shoaling are allowed. The OBC is applied along wave ray characteristics which intersect the open boundary obliquely. The numerical implementation employs Lagrange interpolations in two dimensions from information on a regular grid in the interior region Test results indicate that the numerical boundary is highly transparent to incident waves in the absence of bottom topography. Weak dispersion effects (Airy dispersion, Poincaré dispersion and nonlinear dispersion) are faithfully reproduced in the test simulations The effects of topography (reflection, refraction, and diffraction), which are not included in the OBC, result in some contamination of the solutions. However, the first few leading waves are free from serious error. Also the contamination due to topography near the open boundaries is sporadic and does not produce a cumulative effect. The modified OBC is shown to be a very significant improvement over the simple nondispersive Sommerfeld radiation condition.

1. INTRODUCTION

For real-time prediction of a far-field tsunami signal by a numerical propagation model, accuracy and efficiency are important. To achieve reasonable efficiency, a limited-domain model with an open boundary condition (OBC) is often employed in studies of tsunami propagation (e.g., Hwang *et al.* [1]; Brandsma *et al.* [2]; Kim [3]). An (ideal) OBC is a computational boundary which allows disturbances in the interior domain to be radiated without distortion or spurious reflection. Such boundary conditions are of fundamental importance in fluid dynamics, especially in the areas of oceanography and meteorology.

Since the 1950's OBCs have been studied by several authors including Orlanski [4], Camerlengo and O'Brien [5] and Chapman [6]. Most OBCs are based on the first-order Sommerfeld radiation condition

$$\phi_t + C\phi_s = 0, \tag{1}$$

* Present address: Applied Research Corporation, ARC Technologies, 305 Arguello Drive, College Station, Texas 77840.

0021-9991/88 $3 00

581 76 2-7

where subscripts denote partial differentiation, s the independent variable in the direction of the wave ray characteristics, C the celerity, and ϕ is the water level anomaly or velocity. Different OBCs have different numerical prescriptions for the celerity.

It will be shown that OBCs based on (1) are not sufficiently accurate for studying long-range tsunami propagation. In order to recover a reliable far-field tsunami signal, both the interior governing equation (IGE) and the OBC should allow for the modification of the tsunami wave. The modification factors are (1) energy scattering and concentration by geometry of the source and of the geoid, and bottom topography including reflection, refraction, and diffraction, (2) phase dispersion, considering both the vertical acceleration of the fluid and the rotation of the earth, (3) amplitude dispersion due to nonlinear effects. Unless these (possibly small) effects are properly resolved in an OBC, spurious reflection from the open boundaries might contaminate the interior solution and the real modification of the tsunamis would be obscured. Emphasis is focused on the accurate resolution of the weak dispersion effects which can cause cumulative distortion of the wave signal for long-range propagation.

The main interests in this study are as follows:

(1) development of an OBC consistent with a two-dimensional, dispersive, nonlinear propagation model over an ocean of variable depth,

(2) numerical implementation of the developed OBC, and

(3) tests of the transparency of the OBC for a range of selected conditions.

The model employed in this study, including the IGE, is that developed by Kim [3] and is briefly described in Section 2. The associated OBC is discussed in detail in Section 3. The results of numerical simulations for the selected tests appear in Section 4, followed by a summary and concluding remarks in Section 5.

2. The Numerical Model

Based on the Hamiltonian-action variational principle, the following Boussinesq-type continuum equation governing the evolution of the water level anomaly (η) can be derived:

$$\underset{\text{A}}{\eta_{tt}} - \underset{\text{B}}{g\nabla\cdot(h\nabla\eta)} = \underset{\text{C}}{-f^2\eta} + \underset{\text{D}}{\tfrac{1}{3}\nabla\cdot(h\nabla(h\eta_{tt}))} + \underset{\text{E}}{\tfrac{3}{2}g\nabla\cdot(h\nabla(\eta^2/h))}, \tag{2}$$

where the subscript t denotes partial differentiation with respect to time, g gravitational acceleration, f the Coriolis parameter, h water depth, ∇ the two-dimensional del operator along a level surface (geoid). Approximations to the Hamiltonian action are made appropriate to $kh \ll 1$ (long waves), $|\nabla h| \ll kh$ (mild bottom slope) and $\eta/h \ll 1$ (small amplitude), where k is the typical wavenumber of the tsunami wave.

The primary balance for very small amplitude waves whose wavelength is of the order of 50 to 500 times the depth is with terms A and B. Such waves are essentially nondispersive. All the terms on the right-hand side of (2) represent dispersion effects. Term C accounts for the effect of the earth's rotation; a balance of A, B, C being the linear Poincaré equation appropriate to very long waves, for which Coriolis acceleration produces weak dispersion. For wavelengths of order 5 to 50 times the depth (in which a significant portion of tsunami energy usually resides), the effect of vertical acceleration of the fluid can produce weak phase dispersion. Term D is a Boussinesq-type approximation for this effect. Finally, the effect of nonlinear (amplitude) dispersion is accounted for by term E. This particular form results from an approximation in the Hamiltonian formulation pertinent to waves propagating primarily in one direction. This is justifiable for the oceanic propagation phase of the tsunami problem, but represents an approximation near the source and in regions of strong reflection, where the disturbance can be more nearly a standing wave. The inclusion of amplitude dispersion can partially offset the phase dispersion effects, particularly for the leading waves of a tsunami wave group, well away from the source.

Term D can be approximated by a fourth-order spatial operator by replacing η_{tt} in D by the first-order approximation given by a balance of A and B. This would allow (2) to be rendered in an explicit finite difference form. However, it was found by Kim [3] that the explicit form for this dispersive governing equation is severely restricted in the range of depths for which it can be applied. Relation (2) as it stands implies that the variable (ϕ) being predicted is (combining A and D):

$$\phi = \eta - \tfrac{1}{3}\nabla \cdot (h\nabla(h\eta)).$$

Numerical implementation in this form requires inversion of the above two-dimensional elliptic equation at each time step to obtain η from ϕ and (while potentially of good stability properties) is quite inefficient.

The adopted numerical version of (2) is a compromise in which term D is split as

$$\tfrac{1}{3}\nabla_\mu \cdot (h\nabla_\mu(h\eta_{tt})) + \tfrac{1}{3}\nabla_v \cdot (h\nabla_v(h\eta_{tt})),$$

where (μ, v) are coordinates indicating respectively the principal direction of propagation (source to receiver) and the transverse direction, while (∇_μ, ∇_v) are (μ, v) components of ∇. If one then replaces η_{tt} by its approximation $g\nabla \cdot (h\nabla\eta)$ in the first term above, a semi-implicit form of (2) is achieved in which the term being predicted is

$$\phi = \eta - \tfrac{1}{3}\nabla_v \cdot (h\nabla_v(h\eta)),$$

whose numerical counterpart is easily inverted to obtain η in terms of ϕ. The resulting adopted governing equation is then

$$\eta_{tt} - \tfrac{1}{3}\nabla_v \cdot (h\nabla_v(h\eta_{tt})) + f^2\eta = g\nabla \cdot (h\nabla\eta) + \tfrac{3}{2}g\nabla \cdot (h\nabla(\eta^2/h)) + \tfrac{1}{3}g\nabla_\mu \cdot (h\nabla_\mu(h\nabla \cdot (h\nabla\eta))). \tag{3}$$

Details of the numerical analog of the adopted governing equation will be found in Kim [3], along with an analysis of its stability properties. Since our present focus is on the OBC, these details are considered beyond the scope of this paper. We mention only that the rendition of all terms in (3) in finite difference form should have a truncation error comparable to that associated with the dispersion effects so that the latter is not masked by numerically induced dispersion. In a centered difference analog of (3), terms of order $(\Delta x)^4$, or equivalently, order $(\Delta t)^4$ are retained, where Δx and Δt are spatial and temporal resolutions of the grids. Without the nonlinear term, the resulting difference equation [3] has a dispersion relation accurate to $O(k^4)$ compared with its continuum counterpart.

3. The Open Boundary Condition

A characteristic-type boundary condition is derived upon reducing the time derivative order of the IGE. For the systematic retention of the important terms in deriving an open boundary condition, (3) is nondimensionalized adopting the following scales:

N_0: typical amplitude of the tsunami wave,

H: mean depth,

L: typical length scale in the direction of the wave propagation,

$L/\sqrt{gH}$: typical time scale of the tsunami wave,

$L_v = L/\vartheta$: length scale associated with the variation of η in the transverse direction,

$L_h = L/\varphi$: length scale associated with the variation of h or equivalently $C(=\sqrt{gh})$.

Since the variation of η in the transverse direction is much smaller than that in the principal direction, ϑ is much less than unity. Also, φ is assumed to be a very small parameter (mild bottom slope).

The nondimensionalization of (3) yields parameters $\varepsilon = N_0/H$, $\delta^2 = (H/L)^2$, and $\varrho = fL/\sqrt{gH}$, which are measures of the importance of nonlinear effects, phase dispersion, and the rotation of the earth, respectively. In the context of the Boussinesq-type governing equation, these parameters are much less than unity. Then to order ε, δ^2, ϱ^2, φ, ϑ^2, and $\vartheta\varphi$, (3) is nondimensionalized as

$$\eta_{tt} + \varrho^2\eta = C^2\frac{\partial^2\eta}{\partial\mu^2} + 2\varphi C\frac{\partial C}{\partial\mu}\frac{\partial\eta}{\partial\mu} + \frac{C^2}{p}\frac{\partial p}{\partial\mu}\frac{\partial\eta}{\partial\mu} + 3\varepsilon\frac{\partial}{\partial\mu}\left(\eta\frac{\partial\eta}{\partial\mu}\right) + \frac{1}{3}\delta^2 C^6\frac{\partial^4\eta}{\partial\mu^4} + \vartheta^2\frac{C^2}{p^2}\frac{\partial^2\eta}{\partial v^2} + 2\vartheta\varphi\frac{C}{p^2}\frac{\partial C}{\partial v}\frac{\partial\eta}{\partial v}, \tag{4}$$

where

(1) Cartesian coordinate system (x, y),

$$\mu = x, \qquad \nu = y, \qquad p = 1$$

(2) polar coordinate system (r, θ),

$$\mu = r, \qquad \nu = \theta, \qquad p = r$$

(3) spherical polar coordinate system (θ, λ, ρ),

$$\mu = R_e\theta, \qquad \nu = R_e\lambda, \qquad p = \sin\theta$$

and R_e is the radius of the Earth. The term of order $\vartheta\varphi$ governs the effect of refraction due to bottom topography. The third term on the right of (4) represents the effects of wave spreading in the absence of bottom topography for a source having $\eta = F(\mu)$ only. The importance of this (geometric) spreading is measured by p_μ/p. In deriving an OBC, p_μ/p is considered small since the boundary is well away from the pole of the coordinate system. In a Cartesian coordinate system, geometric spreading does not occur.

The primary (zeroth order) balance in (4) is given by

$$\eta_{tt} = C^2\eta_{\mu\mu}. \tag{5}$$

Since the term of order φ (associated with the variation of C) is neglected, (5) reduces to

$$\eta_t = -C\eta_\mu, \tag{6}$$

for waves propagating in the positive μ direction. Equations (5) and (6) yield two relations

$$\partial/\partial t = -C(\partial/\partial\mu),$$

$$\int_{t_0}^{t} dt = -C^{-1}\int_{\mu_0}^{\mu} d\mu. \tag{7}$$

The lower limits of integration are found such that water level is undisturbed at (t_0, μ_0). Substitutions based on (7) introduce error of order ε, δ^2, ϱ^2, φ, ϑ^2, $\vartheta\varphi$, p_μ/p (hereafter referred to as the first order) when applied to a generalized governing equation (4). The derivation of an open boundary condition is based on the claim that the error due to the use of (7) can be explained by the first-order terms in (4). In the following discussion, the use of (7) for the first-order terms will not be mentioned explicitly since the error is of order higher than the first.

By employing (7) on the right of (4) and then integrating the resulting equation with respect to t an OBC, aside from the coefficients, is derived in the form

$$\eta_t = -c_1 C\eta_\mu - c_2\varphi C_\mu \eta - c_3 Cp^{-1}p_\mu \eta - c_4 \varrho^2 \int \eta\, dt - c_5 \varepsilon C^{-1}\eta\eta_\mu$$

$$- c_6 \delta^2 C^5 \eta_{\mu\mu\mu} - c_7 \vartheta^2 C^{-1} p^{-2} \int C^2 \eta_{vv}\, d\mu - c_8 \vartheta\varphi C^{-1} p^{-2} \int CC_v \eta_v\, d\mu. \quad (8)$$

The coefficients c_i's are determined such that (8) is accurate up to first order. Differentiation of (8) with respect to t yields

$$\eta_{tt} = -c_1 C\eta_{\mu t} - c_2\varphi C_\mu \eta_t - c_3 Cp^{-1}p_\mu \eta_t - c_4 \varrho^2 \eta - c_5 \varepsilon C^{-1}(\eta\eta_\mu)_t$$
$$- c_6 \delta^2 C^5 \eta_{\mu\mu\mu t} + c_7 \vartheta^2 p^{-2} C^2 \eta_{vv} + c_8 \vartheta\varphi p^{-2} CC_v \eta_v. \quad (9)$$

Using (8), the right side of (9) can be restated in terms of spatial derivatives of η. For example, $\eta_{\mu t}$ in the first term on the right is represented (neglecting higher order terms) as

$$\eta_{\mu t} = -c_1(C\eta_{\mu\mu} + \varphi C_\mu \eta_\mu) - c_2\varphi C_\mu \eta_\mu - c_3 Cp^{-1}p_\mu \eta_\mu + c_4 \varrho^2 C^{-1}\eta$$
$$- c_5 \varepsilon C^{-1}(\eta\eta_\mu)_\mu - c_6 \delta^2 C^5 \eta_{\mu\mu\mu\mu} - c_7 \vartheta^2 p^{-2} C\eta_{vv} - c_8 \vartheta\varphi p^{-2} C_v \eta_v. \quad (10)$$

Finally, (9) is rewritten as

$$\eta_{tt} + (c_1 c_4 + c_4)\varrho^2 \eta = c_1^2 C^2 \eta_{\mu\mu} + (c_1^2 + 2c_1 c_2)\varphi CC_\mu \eta_\mu$$
$$+ 2c_1 c_3 C^2 p^{-1} p_\mu \eta_\mu + 2c_1 c_5 \varepsilon(\eta\eta_\mu)_\mu + 2c_1 c_6 \delta^2 C^6 \eta_{\mu\mu\mu\mu}$$
$$+ (c_1 c_7 + c_7)\vartheta^2 p^{-2} C^2 \eta_{vv} + (c_1 c_8 + c_8)\vartheta\varphi p^{-2} CC_v \eta_v. \quad (11)$$

By matching terms in (11) and (4), the c_i's are determined. The resulting boundary condition in dimensional form is given by

$$\eta_t + \frac{1}{2} f^2 \int \eta\, dt + C\eta_\mu + \frac{1}{2} C_\mu \eta + \frac{1}{2p} Cp_\mu \eta + \frac{3C}{2h} \eta\eta_\mu$$
$$+ \frac{1}{6} h^2 C\eta_{\mu\mu\mu} + \frac{1}{2p^2} C^{-1} \int (C^2 \eta_v)_v\, d\mu = 0. \quad (12)$$

In the absence of the earth's rotation, (12) in a Cartesian coordinate system is essentially equivalent to Eq. (28) given by Kirby *et al.* [7] for waves propagating in one direction on a ray. In integrated form their equation is

$$\eta_t + C\eta_x + \frac{1}{2} C_x \eta + \frac{3C}{2h} \eta\eta_x + \frac{1}{6} h^2 C\eta_{xxx} + \frac{1}{2} C \int C^{-2}(C^2 \eta_y)_y\, dx = 0. \quad (13)$$

The difference is the form of the y-dependent refraction/diffraction term. For strictly

unidirectional propagation in constant depth both (12) and (13) reduce to the KdV equation.

Figure 1 shows the dispersion characteristics of the IGE, the OBC, and the exact linear theory. The dispersion relation is obtained employing $\eta = \exp(ik\mu - i\omega t)$ in the absence of nonlinearity, geometric spreading, and bottom topography, where ω

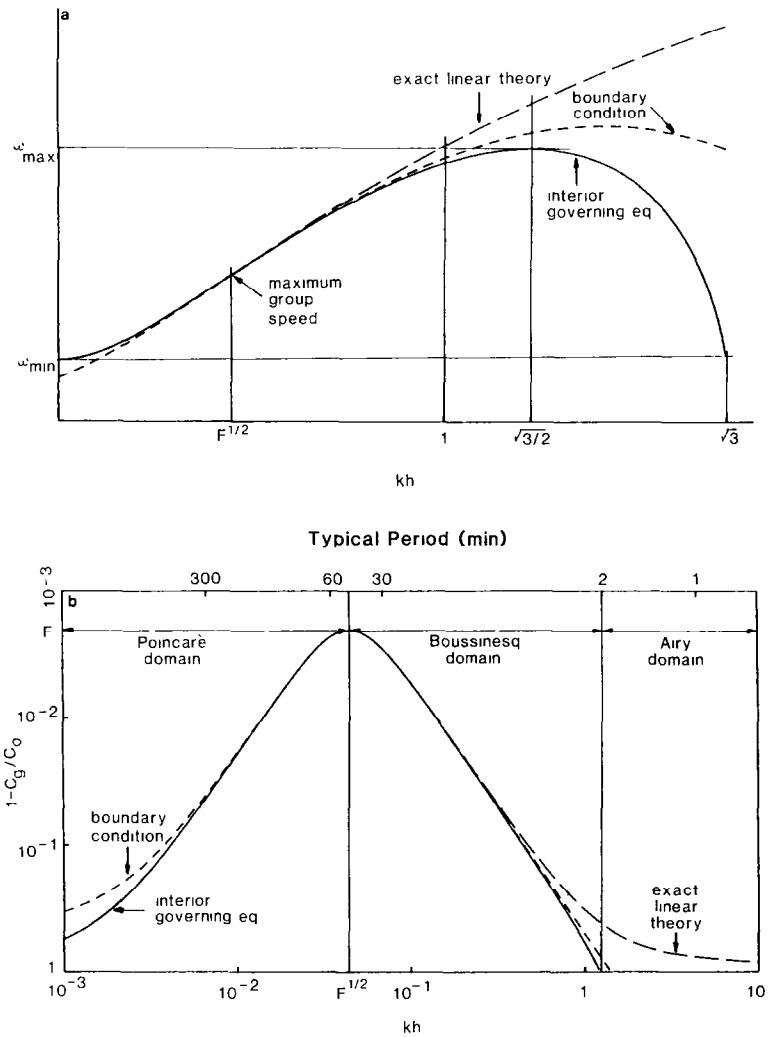

FIG. 1 Dispersion characteristics of the exact linear theory, the linearized version of the interior governing equation, and the lateral boundary condition: (a) ω vs kh; (b) log/log plot of $(1 - C_g/C_0)$ vs kh, where $C_g (= \partial\omega/\partial k)$ and $C_0 (= \omega/k)$ are the group speed and the phase speed, respectively, and $F = f\sqrt{H/g}$. The three domains (from left to right) in the lower figure indicate ranges for the dominance of Poincaré, Boussinesq (weak Airy), and strong Airy dispersion, respectively. The present model is applicable to the range $0.5 \times 10^{-2} < kh < 0.5$

is the frequence. In particular, (12) is differentiated with respect to time to eliminate contribution from the lower limit of integration, which is unimportant for the discussion of the dispersion characteristics. For normal period range of tsunamis (20 min to 2 h), these three dispersion curves are almost coincident. The combined effect of vertical acceleration and the rotation of the earth causes the group speed to have its maximum value at about 50 min period as depicted by Royer and Reid [8]. Without the rotation of the earth, maximum group speed occurs at $k = 0$.

Multiplying (12) by $p^{1/2}C^{1/2}$, an open boundary condition is obtained in a characteristic form as

$$\frac{d\zeta}{dt} = \left\{ -\frac{1}{2} f^2 \int \eta \, dt - \frac{3C}{2h} \eta \eta_\mu - \frac{1}{6} h^2 C \eta_{\mu\mu\mu} - \frac{1}{2p^2} C^{-1} \int (C^2 \eta_\nu)_\nu \, d\mu \right\} (pC)^{1/2} \quad (14)$$

along the path $d\mu/dt = C$, i.e.,

$$\frac{d\zeta}{dt} = \frac{\partial \zeta}{\partial t} + C \frac{\partial \zeta}{\partial \mu}, \quad (15)$$

where $\zeta = \eta p^{1/2} C^{1/2}$. Factors $p^{1/2}$ and $C^{1/2}$ account for the effects of geometric spreading and shoaling, respectively. The terms inside the braces represent the effects of dispersion and of diffraction/refraction. Without such effects, ζ is conserved following any characteristic.

In deriving a discrete form of the OBC, distinction should be made between the two types of coordinate systems adopted in this study—the base coordinate system and the wave coordinate system. At the outset, it is emphasized that the domain of the model is spatially limited by open (computational) boundaries (see Fig. 3). The base coordinate system defines the configuration of a limited domain. The wave coordinate system is defined in regard to the geometry of the source. These two types of coordinate systems need not be same. For example, consider the propagation of waves on a plane geoid by an initial surface displacement of axially symmetric form. Then the wave coordinate system is a polar system with the pole at the center of the initial displacement. The wave coordinate system is suitable for the boundary condition (14) which is solved following the characteristic ray path. At the receiver site, it is desirable to have as dense information as possible. In this respect, a Cartesian system is a proper choice for the base coordinate system. Then the coordinates (μ, ν) in (3) are redefined as (x, y), where $y = 0$ is a line connecting the source and the receiver. Open lateral boundaries are lines along which $y =$ constant. The duality of the coordinate system requires an interpolation in solving (14). In the following, the effects of refraction and diffraction in the OBC are neglected. While such effects are usually small, the error in evaluating the last term of (14) is large in the context of the present model. The difficulty arises primarily due to the fact that the precision of estimates of the derivatives of η transverse to a wave ray near the open boundary is much poorer than that of the derivatives along the ray and this can destabilize the computation.

Equation (14), without the refraction/diffraction term, can be written in a discrete form using upstream differencing (see Fig. 2). That is,

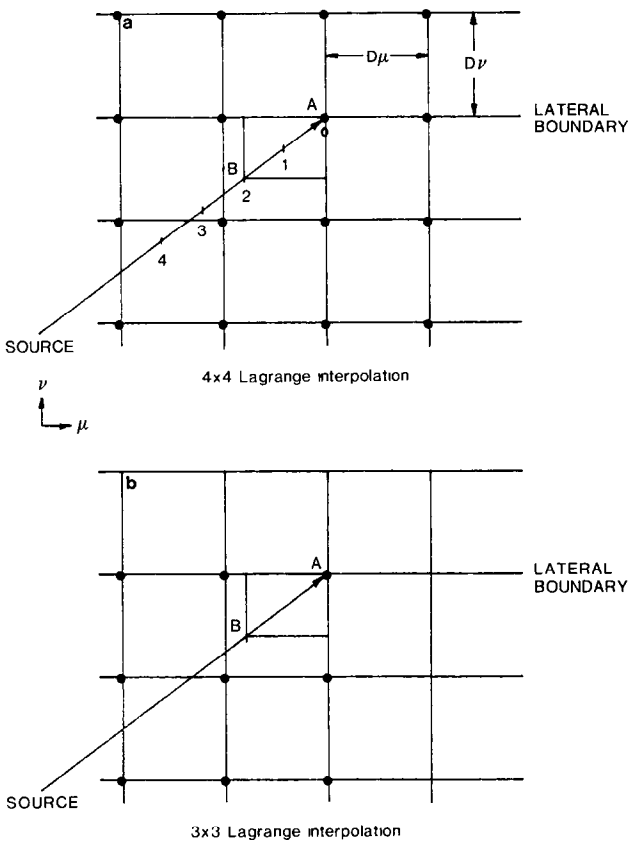

FIG. 2. Schematic figures depicting the interpolation lattice, nodal points (●), interpolation points (numbered 0 to 4 or designated by A and B) and the assumed characteristic ray path (geodesic line joining the source and the point A). (a) 4×4 Lagrange interpolation, (b) 3×3 Lagrange interpolation.

$$\eta_4^{n+1} = \left[\eta^n - \frac{1}{4} (f \Delta t)^2 (\eta^0 + 2\eta^1 + \cdots + 2\eta^{n-1} + \eta^n) - \frac{3}{4h} \Delta(\eta^n \eta^n) \right.$$
$$\left. - \frac{1}{6} h^2 \left\{ \Delta(l^n) - \frac{1}{6} \Delta^3(l^n) \right\} \right]_B (p_B C_B / p_4 C_A)^{1/2}, \tag{16}$$

where A is the point at which the boundary condition is sought, B an interpolation point, n time step, l Laplacian of η, γ the Courant number ($\sqrt{gH}\, \Delta t / D\mu$), $D\mu$ grid size in the μ direction, z scaled depth (h/H), and Δ is a difference operator such that

$$\Delta \eta_B = \eta_1 - \eta_3,$$
$$\Delta^3 l_B = l_0 - 2l_1 + 2l_3 - l_4. \tag{17}$$

So there are actually five interpolation points designated by indices 0 to 4.

Upstream differencing is conducted along the (geodesic) line joining the source and the point A. Without bottom topography, this characteristic path is a wave ray for waves propagating from the source in one direction. With bathymetry, this line is no longer exactly a ray. The determination of the actual ray path is difficult and is not attempted in the present model; we recognize this as a potential source of error. The error is in the assumed angle at which the ray intersects the boundary. The distance between A and B is computed by the local celerity C for given Δt. The time integral term in (14) is evaluated using the trapezoidal rule. The lower limit of integration is set to zero. At this time, the water level anomaly near the open boundary is zero. The $\eta_{\mu_*\mu_*\mu_*}$ term in (14) is approximated by l_{μ_*} and

$$l_{\mu_*}(D\mu_*) = \Delta l - \tfrac{1}{6}\Delta^3 l + O(D\mu_*)^5, \tag{18}$$

where the subscript $_*$ temporarily denotes variables pertaining to the wave coordinate system. According to the previous scale analysis, the addition of $\eta_{\nu_*\nu_*\mu_*}$ $(= l_{\mu_*} - \eta_{\mu_*\mu_*\mu_*})$ does not alter the boundary condition to first order. Using l instead of $\eta_{\mu_*\mu_*}$ is a matter of convenience for the computation.

Each term in (16) is evaluated by a 4×4 Lagrange interpolator. As shown in Fig. 2a, extra points outside the lateral boundary are required for this interpolation. The motivation for such an interpolator is to reduce the error and to stabilize the scheme by placing the interpolation point B near the center of the lattice. In order to compute η's and l's outside the boundary, l's and l^2's (biharmonic) along the boundary need to be known. In other words, if l is known along the boundary, η outside the boundary can be computed using the relation

$$\eta_{i,j+1} = l_{i,j}(D\mu)^2 - \eta_{i,j-1} - \eta_{i+1,j} - \eta_{i-1,j} + 4\eta_{i,j}, \tag{19}$$

where (i, j) are coordinates in the grid system. Radiation equations for l and l^2 are derived by taking spatial derivatives of (14) and neglecting higher order terms (than the truncation error of (14)). These equations are solved using 4×4 and 3×3 Lagrange interpolators, respectively (Fig. 2b).

Numerical damping is inherent for this interpolational scheme. In order to assure that the open boundaries are as transparent as possible, the dispersion properties of (16) and the numerical counterpart of (3) should be matched closely. Accordingly, a small damping is allowed in the interior region in the form

$$\eta^* = \eta + c_1 \Delta_\mu^2 \Delta_\nu^2 \eta + c_2 \Delta_\nu^4 \eta + c_3 \Delta_\mu^6 \eta, \tag{20}$$

where η^* is the filtered solution with $c_1 = 0.076$, $c_2 = 0$, and $c_3 = 0.0096$. The damping coefficients were determined by a numerical experiment designed to optimize the consistency between the dispersion properties of the OBC and the IGE in a Cartesian coordinate system. This damping is a property of the developed model and is different from a real (viscous) damping. Distortion of the solution due to this damping is negligible for the leading waves of the simulated tsunami, as will be shown in the next section.

4. Numerical Simulation Tests

a. *Introduction*

Transparency of the developed OBC is tested under selected conditions for which different effects can be examined individually. For all tests, the source is taken as an initially static surface displacement which has an axially symmetric Gaussian form

$$\eta = \eta_0 \exp(-r^2/2\sigma^2), \tag{21}$$

where r is the radial distance from the source and σ is a measure of the lateral scale of the Gaussian mound. The line joining the center of the Gaussian mound and the receiver is the μ-axis for the computational domain. The initial amplitude η_0 is 100 units, the unit being arbitrary. The Courant number is unity and the grid size $D\mu$ is twice the mean depth H ($=5$ km).

Figure 3 shows the schematic diagram of a limited-domain model. While required bathymetry is stored in a suitably large two-dimensional grid including the source and the receiver, actual computations are carried out over a small subset domain (computational subdomain). The computational subdomain includes the wave front and translates toward the receiver at speed $\sqrt{gH}$, radiating a portion of the wave energy through the lateral and trailing open boundaries, thus accounting for lateral spreading of energy by geometrical dispersion and longitudinal spreading by phase and amplitude dispersions (divergent wave rays centered at the source). At the leading boundary of the computational subdomain the water level is assumed to be undisturbed ($\eta = 0$). This condition is satisfied by placing the initial surface displacement (21) at an appreciable distance (60 $D\mu$ in this study) away from the leading boundary. Since the computational subdomain moves at the mean speed of the front, leading waves cannot overtake the leading boundary on the moving domain. Spurious reflection from the trailing open boundary does not significantly contaminate the solution since the computational subdomain moves at a faster speed than the (short) waves reflected from the trailing boundary. If the lateral

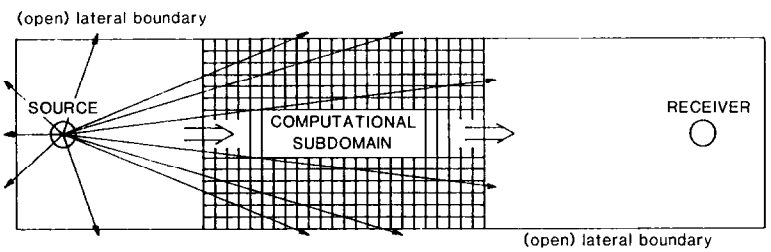

FIG. 3. Schematic grid domain and computational subdomain. The computational subdomain initially includes the source (initial surface displacement) and translates toward the receiver with the wave front. Waves are radiated through the lateral and trailing open boundaries of the computational subdomain. The direction of radiation is determined by the assumed characteristic ray path as shown in the figure. The line joining the source and the receiver is the center (μ-axis) of the domain.

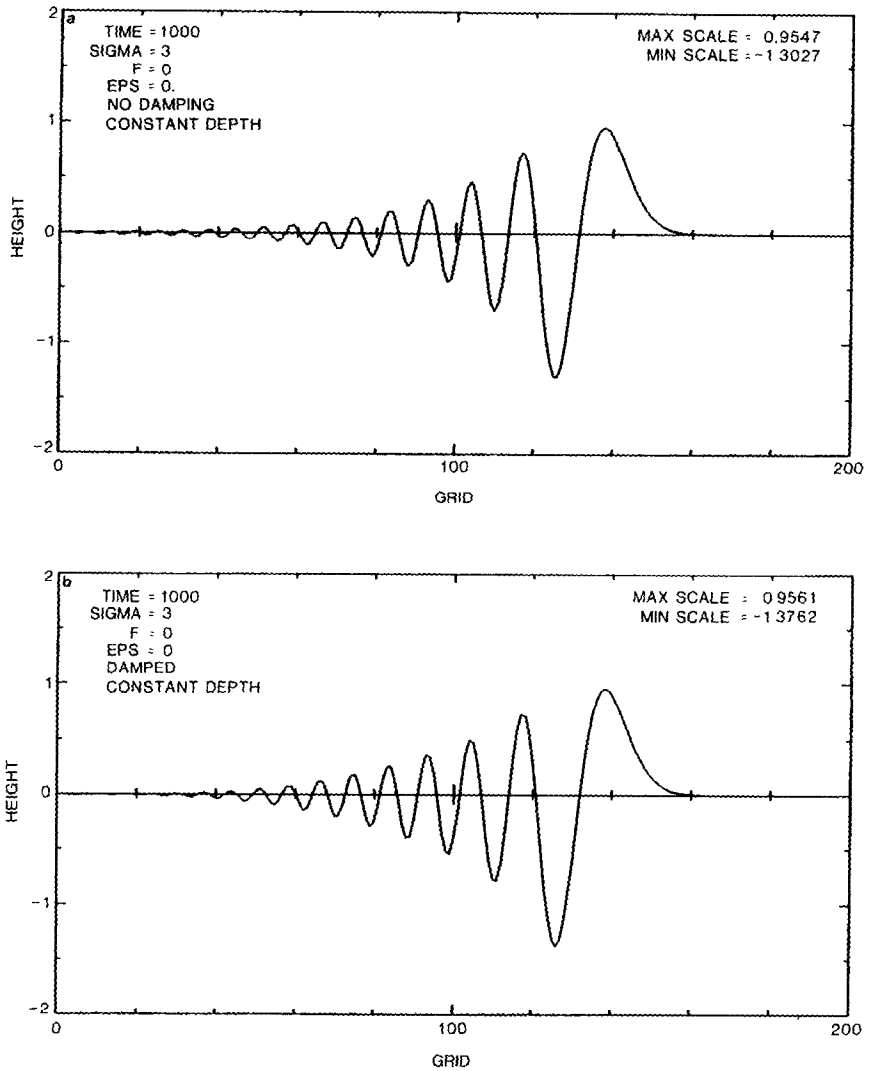

FIG. 4. Water level anomaly along the μ-axis (geodesic line joining the source and the receiver) in the presence of the Airy dispersion effects: (a) analytic r, t model, (b) numerical x, y, t model, (c) numerical r, t model. The initial surface displacement is positioned at 140 on the abscissa. The assumed geoid is a plane. The one-dimensional model adopts a polar coordinate system with the pole at the center of the initial surface displacement. The limited-domain model employs a Cartesian coordinate system. The height scale is in present of the initial surface height (which is 100 units for all tests).

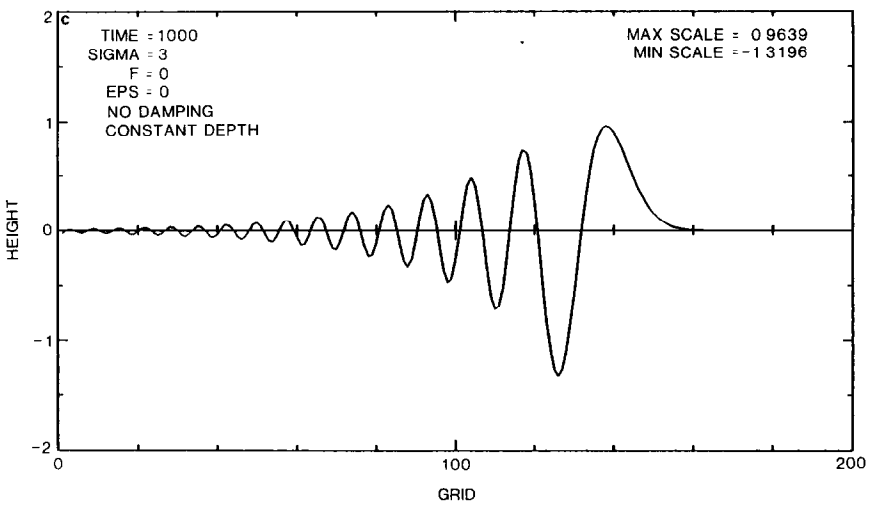

Fig. 4 (*continued*)

boundaries are not transparent, however, spurious reflection may contaminate the leading waves. Thus, the focus here is to examine the transparency of the lateral boundaries where (16) is employed.

The following figures are plots of η along the center (hereafter the μ-axis) of the computational subdomain. Bear in mind that the computational subdomain moves at the mean speed of the wave front. The length (in the μ direction) of the computational subdomain is 200 grid intervals. The initial Gaussian mound was centered at 140 on the abscissa at $t=0$. In the figures, SCALE represents the maximum and the minimum amplitudes of the waves (the original height of the Gaussian mound being 100 units). The scaled parameters TIME, SIGMA, F, and EPS are defined by

$$\begin{aligned} \text{TIME} &= t/\Delta t \text{ (time)}, \\ \text{SIGMA} &= \sigma/D\mu \text{ (lateral scale of the source)}, \\ \text{F} &= f\sqrt{H/g} \text{ (Coriolis parameter)}, \\ \text{EPS} &= N_0/H \text{ (nonlinearity parameter)}. \end{aligned} \tag{22}$$

For simulations with a limited-domain model, SIGMA is set to 3. With larger values of SIGMA, the model is expected to perform better because only a small portion of energy resides in the short-wavelength regime. Note in particular that spurious reflection from the open boundaries is mainly due to short waves as implied in the dispersion curves (Figs. 1a and b). Since all the problems presented are symmetric about the μ-axis, a symmetry condition is employed along the μ-axis. Unless otherwise stated, the lateral width of the domain is 20 grid intervals about the μ-axis.

b. *Test Results with Dispersion Effects in the Absence of Bottom Topography*

The primary interest here is to examine the transparency of the OBC to dispersive wave trains. The effects of reflection, refraction, and diffraction are suppressed by assuming a flat basin. The tests consist mainly of comparing solutions of the limited-domain model (with open boundaries) with analytic solutions and/or solutions of a one-dimensional (1 D) model selected by the geometry of the source and of the geoid. For example, if the initial surface displacement is axially symmetric on a plane geoid in the absence of bottom topography, the problem is essentially one-dimensional if a polar coordinate system is adopted with the pole at the center of the initial displacement. The indeterminacy at the pole when using a 1 D polar model is resolved utilizing L'Hospital's rule. The domain of a 1 D model extends from the pole to infinity without the need of any boundary condition except for the symmetry condition at the pole. Aside from the effects of an OBC (and possibly the truncation error and the indeterminacy at the pole), the limited-domain model and the 1 D model chosen as above are equivalent since both models are based on the same governing equation (3). For the linear, constant depth case, analytic solutions exist for testing the overall numerical model performance. The analytic solutions require a numerical evaluation of the classical integral solution (of Bessel type) to a Cauchy–Poisson problem [3, 9].

The comparison between Figs. 4a and b indicates that the limited-domain model with open radiational boundaries overestimates the maximum $|\eta|$ by about 6 % in the absence of the earth's rotation or the nonlinear effects. Otherwise, the dispersive nature of the solution is produced quite faithfully. This represents a very stringent test of the accuracy of the time marching model with radiational lateral boundaries. Note in particular that for $H = 5$ km, the total propagation distance is 10,000 km. The difference here is a measure of spurious reflection from the open lateral boundaries and, to a lesser extent, the difference in dispersion characteristics of the analytic and numerical renditions of the waves. The difference between Fig. 4a and c is primarily a measure of the difference in dispersion characteristics between the numerical model and the analytic solution.

The comparison between Figs. 5a and b indicates that Poincaré dispersion effects are accurately incorporated in the OBC. For the relatively narrow initial displacement adopted in this study, the effects of the earth's rotation are not pronounced as the difference between Figs. 4a and 5a shows. As the initial displacement becomes wider (as the wavenumber spectrum becomes narrower) the earth's rotation becomes more important, which is implied in the dispersion characteristics (Fig. 1). Table I suggests the possible importance of the Poincaré dispersion for large scale tsunami events at least for long propagation distances.

The comparison between Figs. 6a and b demonstrates that the effects of nonlinear dispersion are faitfully resolved in the OBC. As shown by the profiles given in Figs. 4a and 6a, the nonlinearity incorporated in the present model can significantly offset the phase dispersion and allow greater amplitude of the leading wave compared with the linear case. The decay in amplitude of the leading wave versus

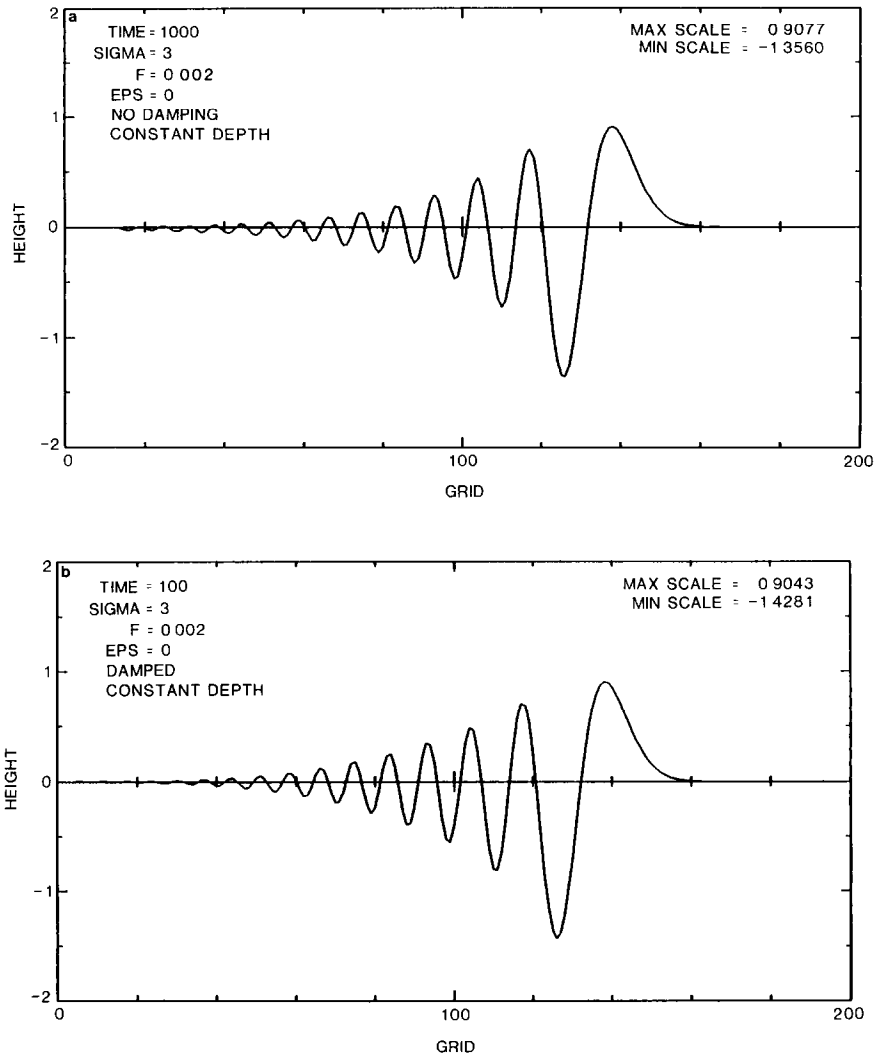

FIG. 5. Same as Fig. 4 except that the effects of the rotation of the earth are added: (a) analytic r, t model, (b) numerical x, y, t model. The scaled value of the Coriolis parameter ($F = 0.002$) is tantamount to $f = 1 \times 10^{-5}$/s for the mean depth of 4 km.

TABLE I

Effect of the Earth's Rotation for Selected Lateral Scales (SIGMA) of the Source at Time Step (TIME) 1000 (linear case)

SIGMA		$F=0.$	$F=0.002$	Differences
3	*A*	0.95	0.91	−0.04
	B	1.30	1.36	0.06
	H	2.25	2.27	0.02
10	*A*	3.60	3.32	−0.28
	B	1.97	2.41	0.44
	H	5.57	5.73	0.16
15	*A*	4.53	4.02	−0.51
	B	2.19	3.03	0.84
	H	6.72	7.05	0.33

Note A = leading positive peak η; B = absolute value of the next peak η; H = range.

time step for different values of the nonlinearity parameter (EPS) is summarized in Fig. 7 for a source with the lateral scale (SIGMA) 3. While the nonlinear parameterization in the model may represent an approximation to the true effect, the major concern here is to examine the transparency of the OBC in the context of the assumed model physics.

c. Test of the Nondispersive Sommerfeld Condition

Test results with dispersion effects show that the dispersive OBC is accurate in the absence of bottom topography. The question remains whether or not the simple Sommerfeld condition (1) would perform equally well. The numerical version of (1) employed in this study is simply (16) without dispersion effects. Nonlinearity and the rotation of the earth are also suppressed in the governing equation. Figure 8 gives the result of a test conducted under the same conditions yielding Fig. 4b but with the nondispersive Sommerfeld condition on the open boundaries. Contamination due to spurious reflection from the open boundaries dominates the numerical solution. Without the added effects of damping, contamination is much worse (not shown here). This test confirms that matching the dispersion characteristics of the OBC with those of the governing equation is highly important for long-range propagation. While dispersion effects contained in the OBC may be small, the error produced by their omission is cumulative.

d. *Test Results with Bottom Topography*

The OBC can accomodate waves propagating only in one direction because the radiational boundary condition is essentially a reduced version of the IGE. Thus the OBC makes no allowance for true reflection by topography near the boundary. Also, since the adopted radiation condition in this study includes no effect of

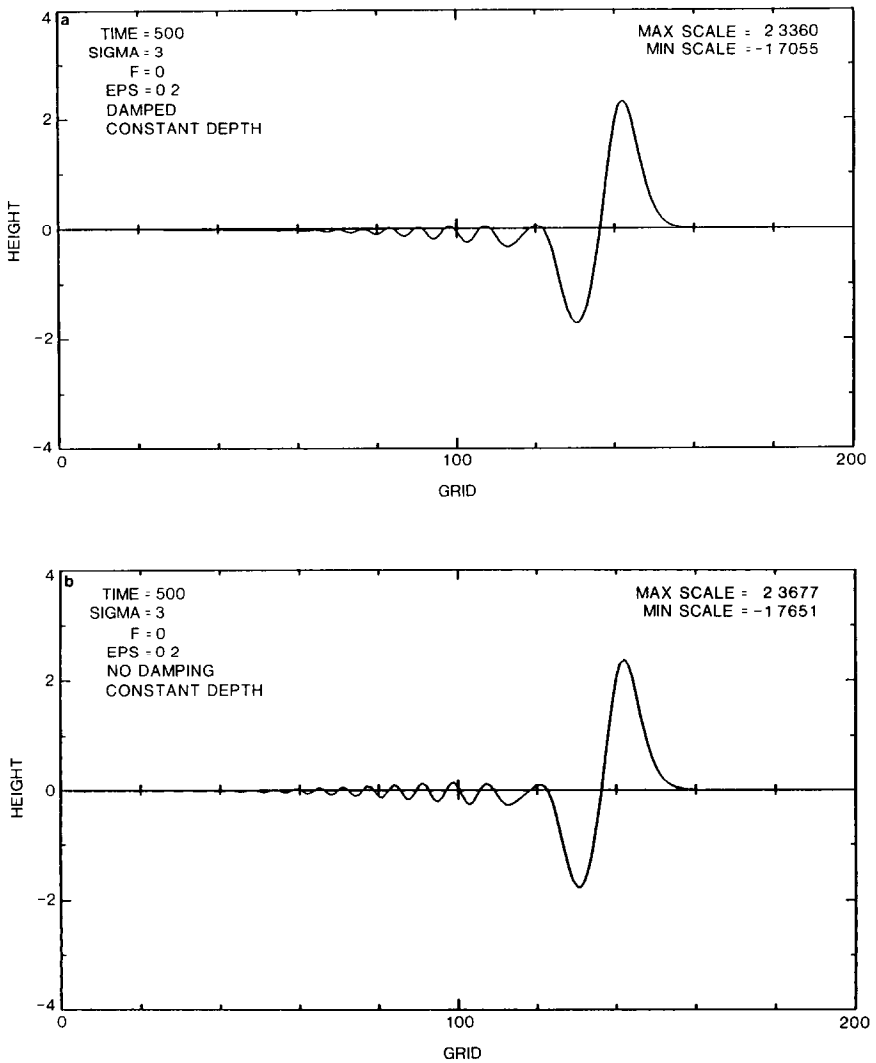

FIG 6. Water level anomaly with Airy dispersion and nonlinear dispersion: (a) numerical θ, t model, (b) numerical θ, λ, t model. The assumed geoid is a sphere. In the one-dimensional model, the adopted coordinate system is a spherical polar system with the pole at the center of the initial surface displacement. The limited-domain model employs the same coordinate system but the north pole is 45° further north of the trailing boundary of the domain.

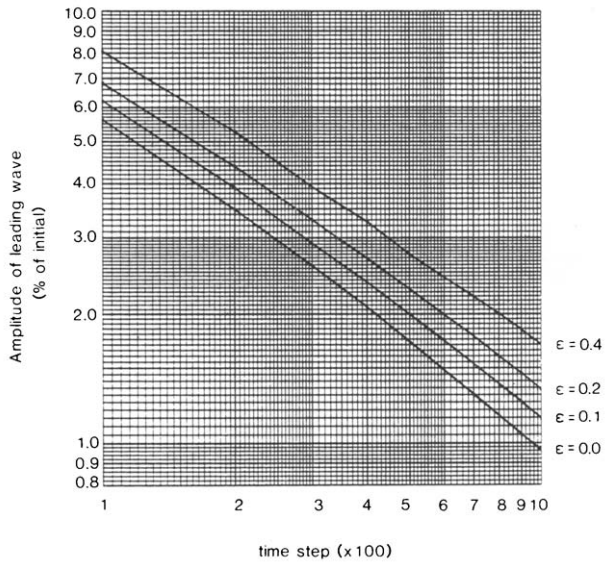

FIG. 7. Amplitude of the leading wave versus time step for selected nonlinearity parameters (EPS, ε) The lateral scale of the source (SIGMA) is 3.

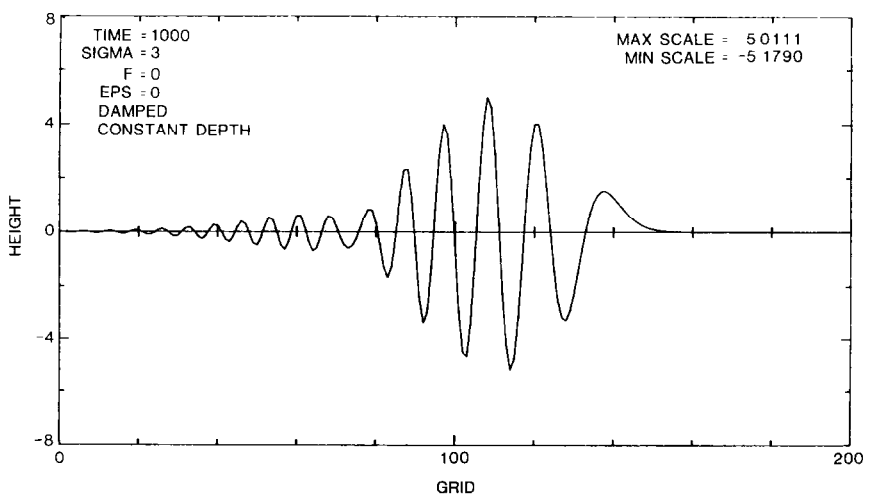

FIG. 8. Water level anomaly employing a numerical x, y, t model as in Fig. 4b with an open boundary condition based on the first-order Sommerfeld equation. The effects of damping are included.

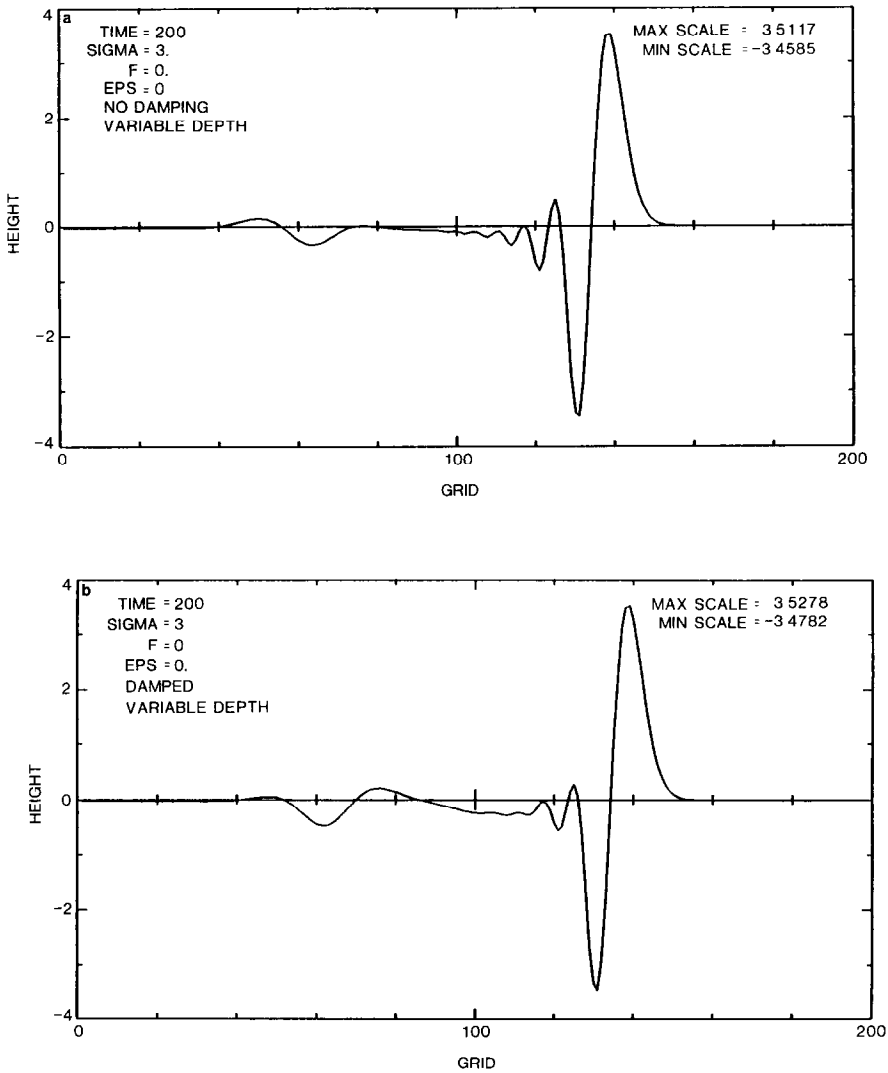

FIG 9. Water level anomaly in the presence of bottom topography which is axially symmetric with respect to the center of the initial surface displacement: (a) numerical θ, t model, (b) numerical θ, λ, t model. The effects of true reflection are shown. Adopted coordinate systems are the same as for Fig. 7.

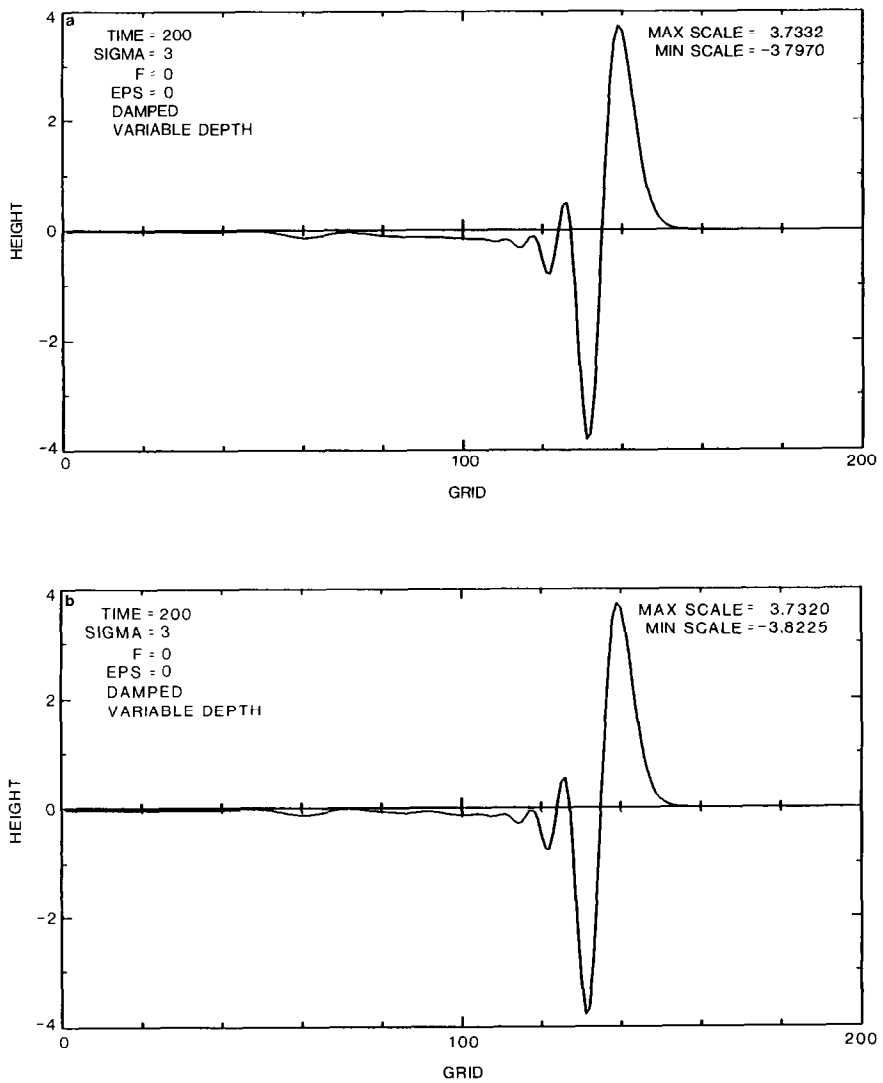

FIG. 10. Same as Fig. 9 but with an isolated bottom topography of axially symmetric Gaussian form. (a) numerical θ, λ, t model with lateral width of 50 grid intervals, (b) numerical θ, λ, t model with lateral width of 20 grid intervals. The effects of refraction/diffraction are shown.

refraction/diffraction, topography inside the domain can contribute to spurious reflection from the open boundaries by changing the angle of radiation.

In order to examine the degree of contamination by true reflections from the lateral boundaries, utilization has been made of the following (scaled) topography:

$$z(r) = 1 - z_0 \exp(-(r - r_z)^2/2\sigma_z^2). \tag{23}$$

Here the constant r_z is the distance from the source to the center of the topographic feature. The effect of refraction is excluded by employing this concentric form of bottom topography with respect to the center of the source. The scaled amplitude z_0 is set to 0.25, $\sigma_z = 3\ D\mu$, and $r_z = 160\ D\mu$.

Comparison of Figs. 9a and b shows that the reflected waves in the trailing portion of the record are contaminated. Also, the amplitudes of the intermediate waves are modified. This is an expected result in view of the reduction in order. It should be emphasized that radiation conditions inherently produce spurious reflections when true reflections exist. The amplitude of the leading wave, however, is relatively free from contamination.

The effects of error in the assumed orientation of wave rays near the boundary, caused by refraction, are examined using an isolated topographic feature of Gaussian form

$$z(r_*) = 1 - z_0 \exp(-r_*^2/2\sigma_z^2), \tag{24}$$

where r_* is the distance relative to the center of this feature. The center is on the μ-axis and is 160 $D\mu$ away from the source. As before, $z_0 = 0.25$, $\sigma_z = 3\ D\mu$. Since a 1D solution no longer is available, the comparison is between the two solutions of the limited-domain model; one is computed over a domain with larger lateral dimension than the other (50 grid intervals compared to 20 grid intervals about the μ-axis). Based on travel time considerations, the solution computed over a larger domain is influenced less by spurious reflections from the open boundaries at least in the leading and middle portions of the wave record. The profiles in Figs. 10a and b show that the effects of refraction are relatively small. Note that there is no true reflection from the open boundaries since the topographic feature is purposely confined to the interior region.

5. Summary and Concluding Remarks

The aim of this investigation was to implement an open boundary condition for weakly dispersive tsunami waves. The developed OBC was tested for transparency under selected conditions which focuses on its sensitivity to various sources of error. Testing of the OBC could be carried out for different initial displacements, topographic features, etc. The degree of contamination could also be examined using different size domains. The tests employed in this study are not intended to be exhaustive, but rather to provide a demonstration that the incorporation of dispersion effects in the OBC can be important.

In implementing the discrete version of the OBC, it is vital to match the dispersion characteristics of the boundary condition with those of the discrete version of the IGE. In this study, small damping was allowed in the interior domain in the fine tuning of this matching. The parameterization of the damping in this study was determined based on a numerical experiment. Such matching is necessary to prevent numerical (spurious) dispersion from obscuring true dispersion effects and is a key to the transparency of the OBC.

It is to be stressed that an accurate OBC is essential for a limited-domain tsunami model, especially when the propagation distance (or time) is large. For a long-range tsunami propagation, dispersion effects may produce significant modification of the waves. In the test, the dispersion effects—vertical acceleration, rotation of the Earth, and nonlinear steepening—are faithfully reproduced in the absence of bottom topography. The degree of error by such effects is less than 6 % in terms of the maximum amplitude of the waves after 1000 time steps (≈ 10 h).

The neglected effects of topography—true reflection, refraction and diffraction—in the OBC produce spurious reflections from the open boundaries, which contaminate the interior solution primarily in the middle and the trailing portions of the wave record. The leading few waves are relatively free from distortion. Since one of the purposes of using a limited-domain model with open boundary condition is to determine the first few leading waves without significant error, it is expected that realistic topography would not impose serious problems. Also it should be emphasized that contamination due to the neglected effects of topography in the OBC is rather sporadic while that due to improper handling of the dispersion effects is cumulative throughout the simulation.

ACKNOWLEDGMENTS

This research was supported by the National Science Foundation under Grant CEE 83-17498. Valuable suggestions from the reviewers were incorporated into the final version of the paper. The authors are particularly grateful for the suggested comparison test using the simple Sommerfeld condition

REFERENCES

1 L. S. HWANG, H. L BUTLER, AND D. J DIVOKY, *Bull. Seismol. Soc. Amer.* **62**, 1579 (1972).
2. M. BRANDSMA, D J. DIVOKY, AND L S. HWANG, Final Report, Tetra Tech, Inc., 1975 (unpublished).
3. K. Y. KIM, Thesis, Texas A & M University, 1986 (unpublished).
4. I. ORLANSKI, *J Comput. Phys.* **21**, 251 (1976).
5. A. L. CAMERLENGO, AND J. J. O'BRIEN, *J. Comput. Phys.* **35**, 12 (1980).
6. D. C. CHAPMAN, *J. Phys Oceanogr.* **15**, 1060 (1985).
7 J. T. KIRBY, P. L. F. LIU, S. B. YOON, AND R. A. DALRYMPLE, in *Proceedings, Nineteenth International Conference on Coastal Engineering, Houston, TX, 1984*, edited by B. L. Edge (American Society of Civil Engineers, New York, 1984), p. 999.
8. T C. ROYER AND R. O. REID, *Tellus* **23**, 136 (1971).
9. P. H LEBLOND AND L. A. MYSAK, *Waves in the Ocean* (Elsevier, New York, 1980), p. 463.